

# NICI Technical Memorandum

SDN 1009

Memo Number: 01:02

**Date:** June 11, 2001

**Subject:** NICI Detector Focus Requirements

**Author:** C. Ftaclas

## **Distribution:**

**Summary:** This memo examines the effects of a focus error at the NICI  $f/36$  (detector) focal plane. Image quality arguments suggest a focus requirement of  $\pm 2\text{mm}$  with a goal of  $\pm 1\text{mm}$  of detector motion. Analysis of various imaging scenarios shows that keeping detector motion within these bounds does not impact coronagraph performance and focal plane differencing.

## **1. Introduction.**

NICI's multiple focal and pupil planes give rise to several different kinds of focus requirements. The top-level external constraints on system focus are:

- a. NICI must be in focus when the location of the telescope focus is constrained to be within  $\pm 1\text{mm}$  absolute relative to a telescope fiducial. 200mm below ISS mounting Plate
- b. NICI must be, minimally, a high quality, high-resolution camera.
- c. For a neutral split, NICI's two focal planes must be differenced to better than one part in a hundred.
- d. NICI instrument focus must be within the baseline focus limits of the AO system
- e. NICI coronagraphic performance must be limited by the telescope + atmosphere.

This memo examines consequences of focus errors within the instrument itself. Possible focus errors within NICI can arise between the first focus and the pupil image, and between the pupil and each of the two imaging channel detectors. The latter effect is the subject of this memo, which addresses the need for a focus mechanism on one or both of the detectors.

## 2. Analysis

Looking at the top level imaging requirements above it is clear that focus errors at the two detector channels can impact more than one of them. Focus errors can:

- a. Degrade image quality.
- b. Degrade coronagraphic performance
- c. Limit our ability to difference the two focal planes.

### a. Image quality.

The most meaningful image quality metric for our application is Strehl, which measures the degradation of the image peak intensity relative to the diffraction-limited case. In the Appendix the **wave-front** error and rms spot size resulting from a focus shift are given. These results can be found in many texts but the results in the Appendix include the effects of arbitrary inner and outer Lyot stops.

For a focus shift of  $dF$ , the resulting rms **wave-front** error is (Eq. A.6):

$$s = \frac{dF}{8f_{\#}^2} \frac{r_L^2 - e_L^2}{\sqrt{12}}$$

where  $f_{\#}$  is the focal ratio and  $r_L$  and  $e_L$  are the normalized outer and inner radii for any Lyot stop that may be present. From the quadratic dependence on focal ratio, it is clear that our focus tolerance is significantly better at the  $f/36$  detector focus than it is at the  $f/16$  telescope focus. This is particularly true when one takes into account the quadratic dependence of scatter on wave front error.

In most situations, the effect of a telescope obscuration is small but in a coronagraph the effect of the Lyot stop can be significant because it limits the radial domain over which an aberration can vary, thus significantly reducing the rms wave-front error. In the absence of a Lyot stop, the factor  $(r_L^2 - e_L^2)$  is  $(1 - 0.16^2) = 0.97$  but for a typical Lyot stop it would be  $(0.9^2 - 0.26^2) = 0.74$ , or only  $\frac{3}{4}$  of its original value. Since scatter varies quadratically with wave front rms the Strehl losses can be half of their pre-Lyot stop values.

Since we are interested in this section in NICI solely as a camera, we consider the more demanding case of no Lyot stop at all. Appendix B shows two MathCAD worksheets that evaluate focus error and other system parameters at both the  $f/16$  and  $f/36$  focal planes. Summarizing these results, 0.062 waves ( $@ I = 2.2\text{mm}$ ) of rms defocus wave-front error result from 1mm of defocus at the  $f/16$  telescope focus and 0.012 waves/mm at the  $f/36$  focus. The corresponding Strehl loss factors are also plotted as a function of defocus.

The system was modeled using input wave fronts generated by Malcolm Northcott in order to evaluate the effects of defocus with a more realistic wave front. These wave front maps simulate output from an 85-element curvature system assuming a bright guide star and infinite outer scale. These wave fronts also assume peak atmospheric conditions of  $r_o = 30$  cm in the visible. The results of five different cases are summarized in Table 1 below and the image core structures are plotted in Figure 1. All cases assume a wavelength  $\lambda = 2.2\mu\text{m}$ . In order to better judge the effects of defocus, oscillations in the point spread functions are smoothed in a way that mimics broad banding with a  $\Delta\lambda / \lambda = 0.1$ . The cases are:

1. An ideal wave front with no phase errors
2. An ideal wave front with the detector shifted by 4 mm.
3. An average of four wave front error maps with no defocus
4. An average of four error maps with the detector shifted 4mm beyond focus.
5. An average of four error maps with the detector shifted 4mm inside focus.

Case Number	$\delta f$ (mm)	$\sigma$ (Waves)	Strehl	Notes
1	0.0	0.0	1.0	Ideal Case
2	+4.0	0.05	0.91	Pure Defocus
3	0.0	0.093	0.75	4 Map Average
4	+4.0	0.103	0.70	4 Map Average
5	-4.0	0.108	0.66	4 Map Average

Table 1. Summary of wave-front error and measured Strehl due to detector defocus.

Wave-front Strehl was calculated exactly from its definition as:

$$S = \frac{(W_{real})^2 + (W_{complex})^2}{(Area_{pupil})^2}$$

where the  $W$ 's are integrals over the real and complex parts of the wave front. As shown in Table 1, there is a slight difference in the Strehl factors between cases 4 and 5 above because the AO wave fronts have some intrinsic residual focus. If we look at the average of these two cases, however, and compare it to the Strehl of the error maps with no defocus, we get  $0.68/0.75 = 0.91$ . This is identical to the effects of defocus on the ideal wave front. That is, on average, the effect of defocus is simply a multiplier on wave front Strehl and we can separate the effects of defocus from those of wave-front errors. This is expected from the approximation of wave front Strehl by  $S = e^{-(2ps/\lambda)^2}$  and is confirmed in this case. Note that even though the defocus error is consistent with this equation, the AO wave fronts are not. For Case 3 above, for example, the wave front rms of 0.093 estimates a Strehl of 0.71 but exact calculation give 0.75. Each of the four individual

maps averaged to produce Table 1 gave lower estimates than the exact calculation showed.

The Strehl effects of defocus can be treated as a multiplier that is well predicted by the estimation formula used in the attached MathCAD spreadsheets. Looking at the energy loss plots for the  $f/36$  focus, the Strehl factor improves to 97.5% for a 2mm defocus and is better than 99% for a 1mm defocus. A compromise between physically achievable placements of optical elements and the steep dependence of Strehl on rms error a reasonable defocus requirement would be  $\pm 2\text{mm}$  (0.024  $\lambda$ ) with a goal of  $\pm 1\text{mm}$  (0.012 $\lambda$ ). This will be taken as a working requirement for the instrument and in what follows.

## **b. Coronagraphic Performance and Frame Differencing**

These two issues are related in that if the frame differencing of the two focal planes is unaffected by defocus then so is coronagraphic performance at any one of them. One difference is that coronagraphic performance is affected by absolute defocus whereas frame differencing depends on the relative defocus between the two focal planes. In order to accommodate both cases we will continue to work with a relative defocus of 4 mm. Because of the symmetry of the effects of defocus, this is a more demanding case than each focal plane being out of focus by 2mm with opposite sense.

The NICI coronagraph design assures that telescope and residual atmospheric phase errors limit the intensity at the second focus. Aberrations within the instrument, like defocus, could limit the performance of the instrument. This is unlikely for the small focus error of 0.024 waves generated by the allowed focus error of 2mm at the detector. Speckles, rather than diffraction, will dominate the image at the final focus. Motion of the detector simply produces defocused speckle images that are smoothed naturally by atmospheric turbulence.

Figures 2 and 3 illustrate the minimal effects of defocus on the structure of the image at the detector. Figure 2 shows the ratio of the intensities at the final focus with and without a focus error. The two cases shown are: one detector perfectly positioned and the other displaced by 4mm, and each detector displaced by 2mm in opposite directions. Plotted are azimuthally averaged intensities using only one atmospheric phase map. In both cases, the difference is just a few percent over most of the focal plane. The ratio of the intensities at the first to the second NICI focus is essentially the coronagraphic gain. Figure 3 shows the log of this gain factor for re-imaged focal planes with (3a) and without (3b) 4mm of defocus, again using just one simulation. There is little difference in the structure of the focal plane intensity. These simulations used a basic coronagraph design with a Gaussian occulting mask (half power point of 0.45 arcsec and a Lyot stop with transmission from 0.26 to 0.9 of the pupil radius).

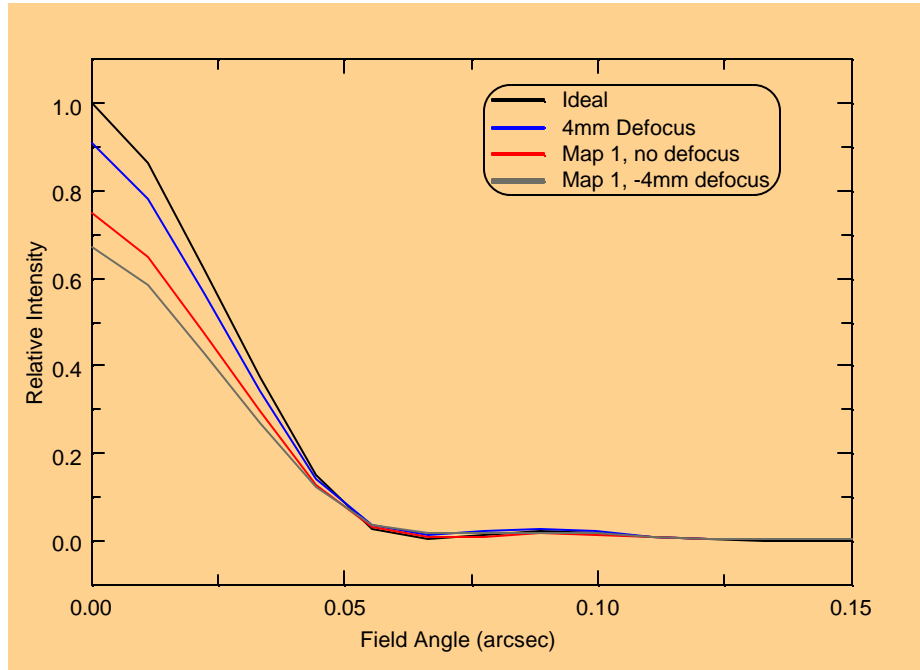


Figure 1. Representative image core structures for various defocus scenarios. The plotted curves correspond to Cases 1, 2, 3 and 5 summarized in Table 1.

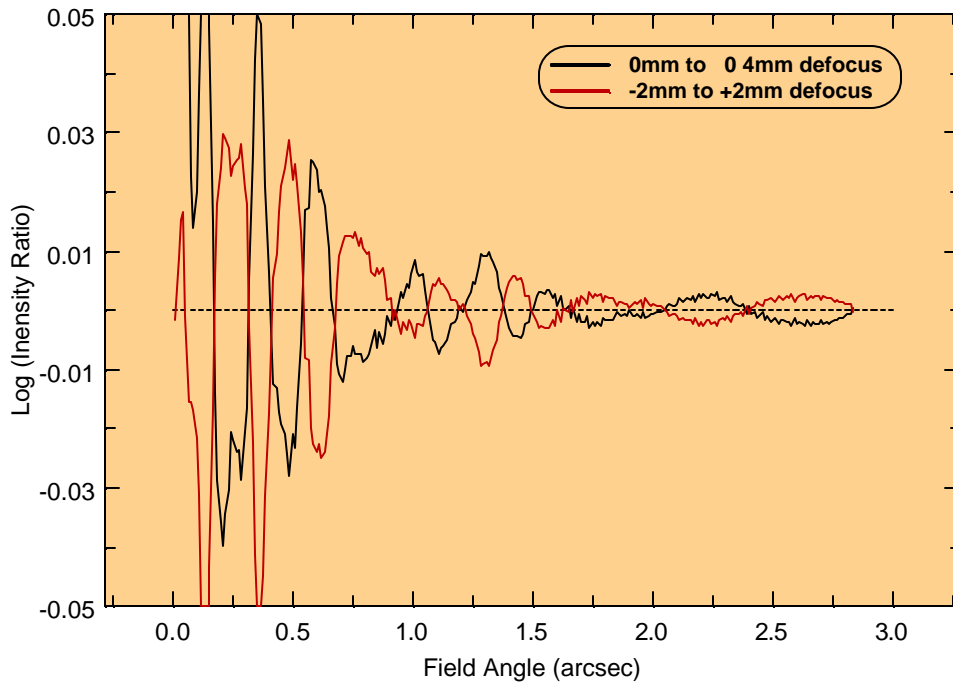


Figure 2. Log ratio of the final focal plane intensities with and without 4mm of relative defocus distributed in two different ways.

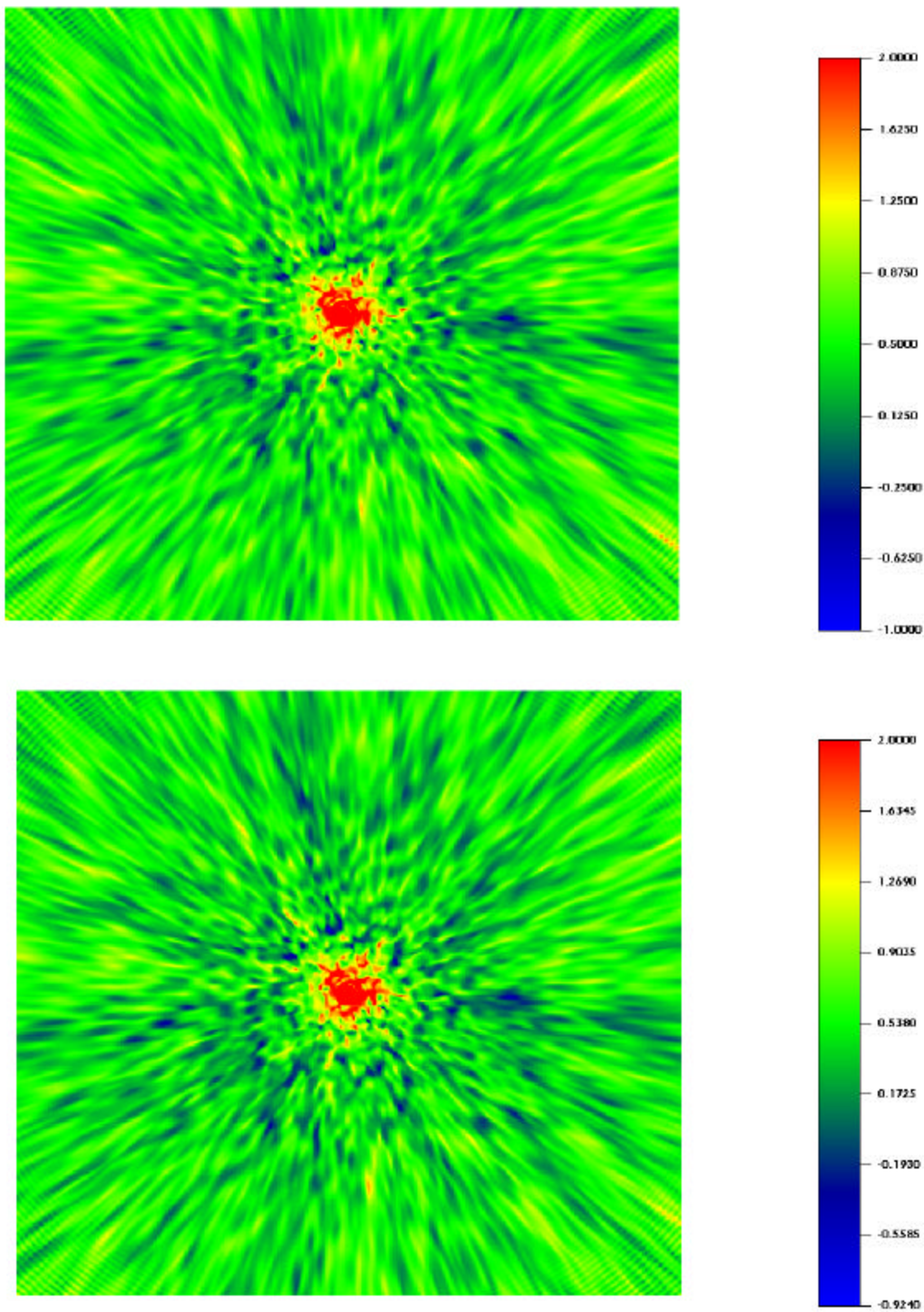


Figure 3 The coronagraphic gain with no focus error (a, top) and with 4mm of defocus (b, bottom). The plotted region is about 5 arc seconds across.

## Appendix A: Treatment of Focus Errors.

Assume we have a perfect spherical wave-front converging to the point  $(0,0,F)$  where  $F$  is the focal length. Any point on the wave-front satisfies:

$$r^2 + (z - F)^2 = F^2, r^2 = x^2 + y^2 \quad (\text{A.1})$$

The height of the wave-front,  $z$ , is then:

$$z = F - \sqrt{F^2 - r^2} \approx \frac{r^2}{2F} \quad (\text{A.2})$$

A defocused wave-front is one that is converging to the point  $F'$  and obeys  $z' = r^2 / 2F'$  the difference between these two wave-fronts is the focus error:

$$\begin{aligned} dz &= z' - z \\ &= \frac{r^2}{2} \left( \frac{1}{F'} - \frac{1}{F} \right) \end{aligned} \quad (\text{A.3})$$

Using  $dF = F' - F$  we get:

$$dz = -\frac{r^2}{2F^2} dF \quad (\text{A.4})$$

The negative sign follows from the fact that the wave-front needs to be flatter than ideal in order for its focal length to increase. The units of  $dz$  are those of  $dF$ . If  $R$  is the overall radius of the wave-front or optic, the focal ratio,  $f_{\#}$ , is  $2R/F$  and the wave-front error due to defocus can be written:

$$dz = -\frac{r^2}{8f_{\#}^2} dF, r = \frac{r}{R} \quad (\text{A.5})$$

Given the phase error, we can evaluate its root mean square value as:

$$s = \frac{dF}{8f_{\#}^2} \frac{r_L^2 - e_L^2}{\sqrt{12}} \quad (\text{A.6})$$

where  $r_L$  is the fractional radius of the outer Lyot stop and  $e_L$  is fractional radius of the inner Lyot stop. At the first focus or in the absence of a Lyot stop, Equation (A.6) becomes:

$$s = \frac{dF}{8f_{\#}^2} \frac{1 - e^2}{\sqrt{12}} \quad (\text{A.7})$$

where, as usual,  $e$  is the linear obscuration ratio of the entrance pupil.

We can now re-express the wave-front error in terms of its rms value:

$$\mathbf{d}_z = -\frac{\mathbf{s}\sqrt{12}}{1-\mathbf{e}^2}\mathbf{r}^2 \quad (\text{A.8})$$

We can also estimate the broadening effects of defocus. At a distance  $\mathbf{d}F$  the height of a ray originating at radius  $r$  in the pupil is given by:

$$\begin{aligned} h &= \frac{r}{F}\mathbf{d}F \\ &= \frac{\mathbf{d}F}{2f_{\#}}\mathbf{r} \end{aligned} \quad (\text{A.9})$$

This allows evaluation of the rms spot size due to defocus as:

$$\mathbf{d}s = \frac{\mathbf{d}F}{2f_{\#}}\sqrt{\frac{1+\mathbf{e}^2}{2}} \quad (\text{A.10})$$

As expected, the rms spot size increases with increasing obscuration ratio and approaches  $R$  as  $\mathbf{e} \rightarrow 1$ . It appears as if the wave-front error has a steeper dependence on focal ratio than the spot size but if we scale the spot size to a meaningful dimension in the focal plane like the diffraction scale,  $s_I = \mathbf{I}f_{\#}$  we get:

$$\frac{\mathbf{d}s}{s_I} = \frac{\mathbf{d}F}{2\mathbf{I}f_{\#}^2}\sqrt{\frac{1+\mathbf{e}^2}{2}} \quad (\text{A.11})$$

which has the same dependence on  $f_{\#}$  as the wave-front error.

## **Appendix B. NICI Defocus Worksheets**

**The following two Mathcad worksheets describe the effects of wave-front errors at the  $f/16$  telescope focus and the  $f/36$  instrument final focus.**

**Gemini Defocus Worksheet: Calculates the effects of a focus shift in terms of wavefront error, image size and Strehl.**

**User Input:**

Telescope Diameter:  $D := 7.9$  meters  
 Telescope Obscuration:  $\epsilon := 0.16$   
 Operating Wavelength:  $\lambda := 2.2$  microns  
 Focal Ratio:  $f_{no} := 16.$

**Relevant Equations:**

Airy  $:= \lambda \cdot f_{no}$       Airy = 35.2      Ring width in microns

$$\sigma(\delta F, f_{no}, \epsilon, \lambda) := \frac{1000 \cdot \delta F}{8 \cdot \lambda \cdot f_{no}^2} \cdot \frac{(1 - \epsilon^2)}{\sqrt{12}} \quad \sigma(1, f_{no}, \epsilon, \lambda) = 0.062$$

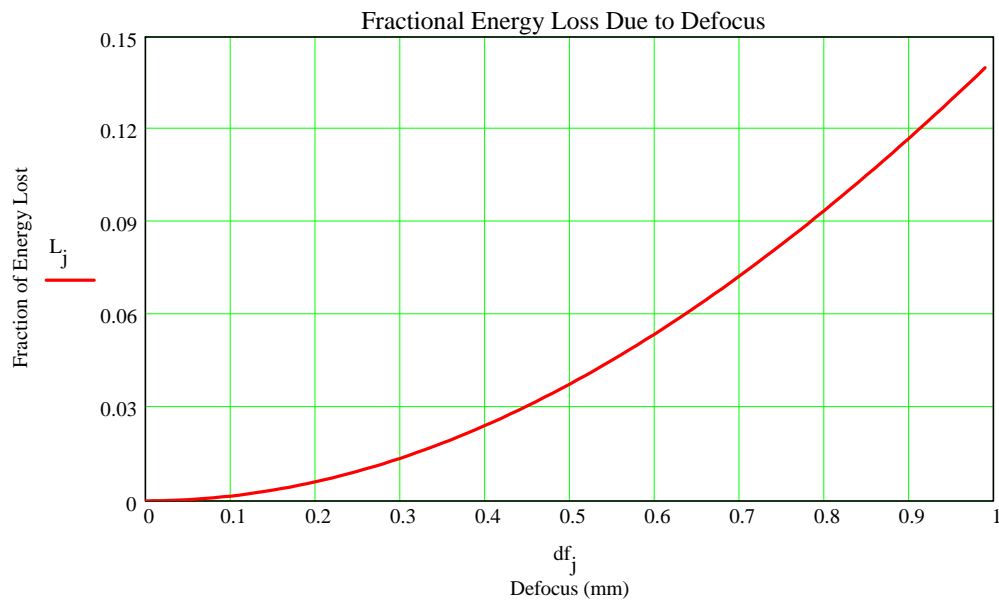
Waves rms wavefront per mm of defocus.

$$\delta s_{rel}(\delta F, f_{no}, \epsilon) := 1000 \cdot \frac{\delta F}{f_{no}} \cdot \sqrt{\frac{1 + \epsilon^2}{8}} \quad \delta s_{rel}(1, f_{no}, \epsilon) = 22.378$$

RMS spot radius per mm of defocus (microns)

$$\frac{\delta s_{rel}(1, 36, \epsilon)}{\text{Airy}} = 0.283 \quad = \text{geometric spot size over diffractive spot size } (\delta F=1\text{mm}).$$

$$S(\delta F, f_{no}, \epsilon, \lambda) := \exp\left[-(2 \cdot \pi \cdot \sigma(\delta F, f_{no}, \epsilon, \lambda))^2\right] \quad j := 1..10 \quad df_j := \frac{(j-1)}{100} \quad L_j := 1 - S(df_j, f_{no}, \epsilon, \lambda)$$



**Gemini Defocus Worksheet: Calculates the effects of a focus shift in terms of wavefront error, image size and Strehl.**

Telescope Diameter:  $D := 7.9$  meters  
 Telescope Obscuration:  $\epsilon := 0.16$   
 Operating Wavelength:  $\lambda := 2.2$  microns

**User Input:**

Focal Ratio:  $f_{no} := 36.$        $36 \cdot 2.2 = 79.2$        $\frac{1}{72} = 0.014$   
 $.126 \cdot 80 = 10.08$

**Relevant Equations:**

Airy :=  $\lambda \cdot f_{no}$       Airy = 79.2      Airy Ring width in microns

$$\sigma(\delta F, f_{no}, \epsilon, \lambda) := \frac{1000 \cdot \delta F}{8 \cdot \lambda \cdot f_{no}^2} \cdot \frac{(1 - \epsilon^2)}{\sqrt{12}} \quad \sigma(1, f_{no}, \epsilon, \lambda) = 0.012$$

Waves rms wavefront per mm of defocus.

$$\delta s_{rel}(\delta F, f_{no}, \epsilon) := 1000 \cdot \frac{\delta F}{f_{no}} \cdot \sqrt{\frac{1 + \epsilon^2}{8}} \quad \delta s_{rel}(1, f_{no}, \epsilon) = 9.946$$

RMS spot radius per mm of defocus (microns)

$$\frac{\delta s_{rel}(1, 36, \epsilon)}{\text{Airy}} = 0.126 \quad \text{= geometric spot size over diffractive spot size } (\delta F=1\text{mm}).$$

$$S(\delta F, f_{no}, \epsilon, \lambda) := \exp\left[-(2 \cdot \pi \cdot \sigma(\delta F, f_{no}, \epsilon, \lambda))^2\right] \quad j := 1..10 \quad df_j := \frac{(j-1)}{25} \quad L_j := 1 - S(df_j, f_{no}, \epsilon, \lambda)$$

